Analytical Methods

PAPER

View Article Online
View Journal | View Issue

Cite this: *Anal. Methods*, 2018, **10**, 4170

A sensitive label-free FRET probe for glutathione based on CdSe/ZnS quantum dots and MnO_2 nanosheets†

Yueyao Mi, Xiaoxue Lei, Heyou Han, Jiangong Liang and Lingzhi Liu*

Glutathione (GSH) is an important antioxidant and plays crucial roles in basic biological functions. Thus far, it still remains a challenge to develop convenient and reliable ways to quantify and monitor the changes in bodily GSH levels. Herein, we have developed a simple, sensitive, and label-free fluorescence resonance energy transfer (FRET)-based probe for GSH with MnO_2 nanosheets as an energy acceptor and silica coated CdSe/ZnS quantum dots (QDs) as the energy donor. The *in situ* synthesis of MnO_2 nanosheets allowed the direct formation of QDs@SiO_2@MnO_2 nanocomposites, and enabled the occurrence of FRET with the donor fluorescence to be quenched. Upon the addition of GSH, MnO_2 nanosheets were decomposed, and QDs@SiO_2 nanobeads were released with a remarkable recovery of the fluorescence intensity in a target-dependent manner. The established FRET probe showed excellent selectivity and sensitivity towards GSH. The feasibility of the probe for GSH detection in a complex matrix was further investigated by analyzing the GSH content in reduced glutathione tablets. The results indicated the capability of the probe to detect low concentrations of GSH and suggested the practicability of the probe for GSH determination in real samples.

Received 10th July 2018
Accepted 3rd August 2018

DOI: 10.1039/c8ay01532e

rsc.li/methods

Introduction

Glutathione (GSH), a plentiful thiol-containing tripeptide in mammals, plays crucial roles in basic biological functions, including oxidation resistance, scavenging free radicals, and modulating critical cellular processes.[1,2] As GSH is an important antioxidant, the dysregulation of its level is related with many diseases, such as Parkinson's disease,[3] liver disease,[2] Alzheimer disease,[4] and caducity.[5] Although numerous methods have been used to detect trace amounts of GSH, it still remains a challenge to develop convenient and reliable ways to quantify and monitor the changes in GSH levels to further investigate its physiological and pathological functions.

Thus far, many analytical techniques, including electrochemistry assay,[6] surface-enhanced Raman scattering,[7] electrogenerated chemiluminescence,[8] mass spectrometry,[9] fluorescence spectroscopy,[10] and colorimetric assay,[11,12] have been developed and applied to the determination of GSH. Among these strategies, fluorescence techniques have been one of the most extensive methods for their advantages of simplicity, speed, and high sensitivity. To date, a large number of fluorescent probes have been developed for detecting or monitoring trace amounts of GSH *in vitro* and *in vivo*.[13–20] The reported probes were mainly focused on organic dyes,[14] quantum dots (QDs),[15] upconversion nanoparticles (UCNPs),[16] fluorescent graphene quantum dots (GQDs),[17] carbon dots (CDs),[18] and metal nanoclusters (NCs).[19,20] Organic dyes can be commercially available, but most of them are limited by their narrow excitation with broad emission and poor photostability.[21] Although the outstanding features of UCNPs enable non-autofluorescence assays with high photostability, they also have the limitations of high-cost, complicated assay procedures, and overheating effects induced by near-infrared light.[18] Compared to UCNPs, GQDs and CDs are superior because of simple synthesis and low cost; however, their quantum yields require improvement.[22,23]

QDs, known as colloidal nanocrystalline semiconductors,[24] possess many unique features, such as broad absorption bands, size-dependent narrow symmetric emission bands, high quantum yields,[25] and good photochemical stability.[24] Due to their excellent optical properties, QDs have been extensively used in the fields of biosensing,[25] bioimaging,[26] photodynamic therapy,[27] and novel electro-optical devices.[28] It has been reported that overcoating the native core with higher band gap inorganic semiconductor materials can largely improve the photoluminescence quantum yields, chemical stability, and photostability of QDs by passivating the surface nonradioactive recombination sites.[29–31] As a type of core–shell QD, CdSe/ZnS QDs possess the above-mentioned advantages, and are considered to be promising optical labels. According to the literature, CdSe/ZnS QDs have been used as fluorescent probes for the

College of Science, Huazhong Agricultural University, Wuhan 430070, China. E-mail: liulingzhi_1981@mail.hzau.edu.cn; Fax: +86-27-8728-2133; Tel: +86-27-8728-3712

† Electronic supplementary information (ESI) available: Fig. S1–S6. See DOI: 10.1039/c8ay01532e

detection of metal ions,[32,33] small molecular substances,[34,35] proteins,[36] and nucleic acids.[37] Although a variety of biosensors based on CdSe/ZnS QDs have been successfully constructed, there has been an increase in concerns regarding the cytotoxicity correlating with the release of free cadmium ions from the core.[38] In addition, the hydrophobic nature of CdSe/ZnS QDs also restricts their further use in biological applications. An attractive approach to circumvent the aforementioned problems is the utilization of surface modification.

Several surface modification methods involving ligand exchange,[39] coating with amphiphilic molecules,[40] and silanization,[41] have been designed for hydrophobic QDs to enhance their water dispersity and biocompatibility. For instance, Huang *et al.* developed a novel and effective silica coating strategy by direct encapsulation of hydrophobic QDs into silica beads.[41] The results showed that the fluorescence of QDs was highly preserved, and the photostability of QDs in aqueous media was greatly improved. Apparently, silica coating is an effective way to transfer hydrophobic QDs into aqueous phase[42] and reduce their cytotoxicity.[41]

Recently, biocompatible two-dimensional graphene analogues (2D-GAs) with planar topography have attracted much attention in terms of constructing biosensing platforms due to their unique properties that are derived from the ultrathin thickness and 2D morphology.[43] As a class of 2D-GAs, manganese dioxide (MnO_2) nanosheets possess a large surface area and a broad absorption spectrum with a high molar extinction coefficient ($\varepsilon = 1.13 \times 10^4$ L mol^{-1} cm^{-1}),[44] allowing them to be a potential energy acceptor in building fluorescence resonance energy transfer (FRET)-based optical sensing platforms. In 2011, Deng *et al.* proposed the first hybrid FRET system with MnO_2 nanosheets as the energy acceptor and UCNPs as the energy donor for intracellular GSH detection.[16] The results indicated that the quenching was highly efficient, and the detection was very sensitive. Thereafter, several FRET-based sensing platforms with MnO_2 nanosheets as energy quenchers have been constructed. The relevant energy donors involved organic dyes,[45] UCNPs,[46] graphitic-C_3N_4,[47] CDs,[48,49] GQDs,[17] metal NCs,[50,51] QDs,[52,53] MoS_2 QDs,[54] Si QDs,[55] and persistent luminescence nanoparticles (PLNPs).[56]

Enlightened by previous works, a simple, sensitive, and selective label-free FRET-based probe for GSH was constructed using MnO_2 nanosheets as the energy acceptor and rationally designed silica-coated CdSe/ZnS QDs as the energy donor. The principle of the sensing system is illustrated as Scheme 1. To improve the water dispersity and biocompatibility of hydrophobic QDs, a silica coating procedure was conducted firstly to produce QDs@SiO_2 nanobeads. Then, 2-(*N*-morpholino)ethanesulfonic acid (MES) buffer and potassium permanganate ($KMnO_4$) solution were introduced. Under the reduction of $KMnO_4$ by MES, MnO_2 nanosheets were directly formed on the surface of QDs@SiO_2 nanobeads. The *in situ* synthesis of MnO_2 nanosheets allowed the formation of QDs@SiO_2@MnO_2 nanocomposites, and thus, FRET occurred. Once GSH was added, MnO_2 nanosheets were decomposed to Mn^{2+} ions and QDs@SiO_2 nanobeads were released to the solution, resulting in a remarkable recovery of the fluorescence intensity that was dependent on the concentration of GSH. The established FRET probe was facile, stable, and sensitive for quantitative assay of GSH both in aqueous solutions and real samples.

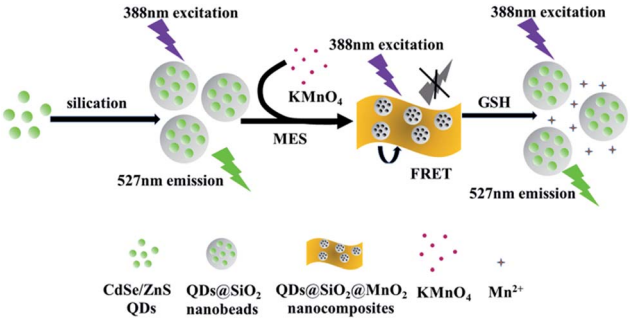

Scheme 1 Schematic illustration of the CdSe/ZnS QDs@SiO_2@MnO_2 nanocomposites-based FRET probe for GSH.

Experimental

Materials

Hydrophobic CdSe/ZnS core–shell QDs (3 mg mL^{-1} in hexane) with alkylamine ligand and a maximum emission wavelength of 525 nm were purchased from Wuhan Jiayuan Quantum Dots Co., Ltd. (Wuhan, China). Sodium silicate solution (27 wt% SiO_2), glutathione (GSH), L-cysteine (Cys), DL-homocysteine (Hcy), and vitamin C were obtained from Sigma-Aldrich (St. Louis, MO, USA). Dodecyltriethoxysilane (DODTEOS) (93%) was from Tokyo Chemical Industry Co., Ltd. (Tokyo, Japan) and 2-(*N*-morpholino)ethanesulfonic acid (MES) was from Biosharp (Hefei, China). Aqueous ammonia (28%), glutamic acid (Glu), proline (Pro), and glucose were from Sinopharm Chemical Reagent Co., Ltd. (Shanghai, China). Reduced glutathione tablets were purchased from Chongqing Yaoyou Pharmaceutical Co., Ltd. (Chongqing, China). All other chemicals were of analytical grade and were used without further purification. All solutions were prepared in ultrapure water with a resistivity of 18.2 MΩ cm.

Instruments

The UV-Vis absorption spectra were recorded on a UV2450 UV-Vis spectrophotometer (Shimadzu Scientific Instruments Inc.) equipped with a 1 cm quartz cell. The fluorescence spectra were measured on a RF-5301PC fluorescence spectrophotometer (Shimadzu Scientific Instruments Inc.) under the excitation of 388 nm with excitation and emission slit widths of 3 nm and 20 nm, respectively. Fluorescence lifetime measurements were performed on an FLS920 steady state and lifetime spectrofluorimeter (Edinburgh Instruments Ltd., UK) under the excitation of 388 nm. Fourier transform infrared (FTIR) spectra were collected on a Nicolet Avatar-330 spectrometer (Thermo Nicolet, USA) using the KBr pellet technique. Hydrodynamic diameters and zeta potential were obtained with a Zetasizer Nano ZS Instrument (Malvern, England). Energy dispersive X-ray spectroscopy (EDS) spectra were measured on a Hitachi SU8010 scanning electron microscope (Hitachi, Japan), and X-ray

photoelectron spectroscopy (XPS) was performed on a VG Multilab 2000 X-ray photoelectron spectrometer (Thermo VG, UK). High-resolution transmission electron microscopy (HRTEM) images were acquired with a JEM-2100F transmission electron microscope (JEOL, Japan) operating at an acceleration voltage of 200 kV.

Synthesis of CdSe/ZnS QDs@SiO_2 nanobeads

CdSe/ZnS QDs@SiO_2 nanobeads were synthesized according to a previous study with small modifications.[41] Briefly, 500 μL of CdSe/ZnS QDs (3 mg mL^{-1}) was mixed with an equal volume of ethanol to precipitate the QDs. The resultant precipitate was collected and dissolved in 20 μL DODTEOS. Organosilane was then added with 20 mL water and 30 μL aqueous ammonia (28%) solution, after which the mixture was treated with a tapered microtip sonicator (VCX800 ultrasonic processor, Sonics) for one hour with 30% amplitude and a 6 mm diameter probe. The working circle was set as 5 s sonicating and 3 s pausing over the period. The resulting solution was filtered with a 0.22 μm pore size filter and mixed with 20 μL sodium silicate solution. After stirring at room temperature for 48 h, the as-prepared CdSe/ZnS QDs@SiO_2 nanobeads were collected and stored at 4 °C for further experiments.

The concentration of QDs in QDs@SiO_2 nanobeads was determined from the absorption spectrum according to a previously reported method.[57]

Preparation of QDs@SiO_2@MnO_2 nanocomposites

MnO_2 nanosheet-modified QDs@SiO_2 nanobeads were prepared using a method analogous to others.[16] Firstly, the molar ratio of MnO_2 nanosheets to QDs@SiO_2 nanobeads was optimized. Different volumes of $KMnO_4$ (1.00 mM) were added to 25 μL of MES buffer (0.10 M, pH 6.0) containing 10 μL of QDs@SiO_2 nanobeads (0.32 μM) and sonicated together for 30 min. Then, the samples were subjected to fluorescence measurements to obtain a final optimal molar ratio. According to the optimized molar ratio (6.40 nM QDs@SiO_2 nanobeads *versus* 0.24 mM MnO_2 nanosheets), 90 μL of QDs@SiO_2 nanobeads (0.32 μM) was added to a centrifuge tube containing 225 μL of MES buffer (0.10 M, pH 6.0). Subsequently, 1080 μL of $KMnO_4$ (1.00 mM) was pipetted to the above tube. The mixture was sonicated for 30 min, and a brown colloid was formed. After centrifugation at 10 000 rpm for 5 min and washing twice with ultrapure water, the obtained QDs@SiO_2@MnO_2 nanocomposites were dispersed in ultrapure water for further use. For comparison, pure MnO_2 nanosheets were also prepared following the same procedure in the absence of QDs@SiO_2 nanobeads.

Detection of GSH

For the GSH detection experiment, varying concentrations of GSH, *i.e.*, 0, 0.010, 0.020, 0.025, 0.050, 0.10, 0.16, 0.20, 0.25, 0.30, 0.35, 0.39, and 0.48 mM, were added to the dispersion of QDs@SiO_2@MnO_2 nanocomposites. After incubating at room temperature for 16 min, the fluorescence emission of QDs@SiO_2 nanobeads was measured under the excitation of 388 nm.

Selectivity studies

To investigate the specificity of QDs@SiO_2@MnO_2 nanocomposites towards GSH, a series of interfering substances was prepared and added to QDs@SiO_2@MnO_2 nanocomposites under the same experimental conditions. The concentrations of Na^+, K^+, Ca^{2+}, Zn^{2+}, Mg^{2+}, and Mn^{2+} were set as 2.00, 2.00, 15.00, 0.10, 0.30, and 2.00 mM, respectively, while the concentrations of Cys, Hcy, glucose, Pro, Glu, vitamin C, and GSH were fixed at 0.10, 0.015, 0.050, 0.050, 0.050, 0.040, and 0.48 mM, respectively.

Treatment with GSH tablets

For the application of pharmaceutical analysis, 5 reduced glutathione tablets were weighed and powdered.[58] After calculating the average weight of each tablet, a certain amount of powder was weighed and added to 8 mL ultrapure water. The obtained mixture was then subjected to an ultrasonic bath for 10 min, followed by centrifugation at 12 000 rpm for another 10 min to remove the insoluble substances. The supernatant was collected and diluted 6 times for further analysis.

Results and discussion

Characterization of QDs@SiO_2 nanobeads

Coating hydrophobic QDs with a silica layer can greatly enhance their water solubility, photostability, and reduce their cytotoxicity.[41] $KMnO_4$ is known as a strong oxidizing agent and may affect the surface of QDs. Therefore, to improve the biocompatibility of QDs and avoid the oxidation by $KMnO_4$, hydrophobic CdSe/ZnS core–shell QDs were modified with a silica layer through organosilane micellization and silicate deposition.

The absorption and fluorescence properties of the starting materials, *i.e.*, the hydrophobic CdSe/ZnS core–shell QDs, were characterized first. As shown in Fig. 1A, the first exciton absorption peak of hydrophobic CdSe/ZnS QDs was found to be 510 nm, with the fluorescence emission peak centered at 525 nm. The emission peak was narrow and symmetric, indicating the good size distribution of hydrophobic CdSe/ZnS QDs. Fig. 1B shows the high resolution transmission electron microscopy (HRTEM) image of hydrophobic CdSe/ZnS QDs. From the figure, it can be seen that the hydrophobic CdSe/ZnS QDs were well dispersed and uniform in shape with an average size of 5.0 ± 1.0 nm.

Retaining the original optical properties of hydrophobic QDs is a big challenge for QDs silication.[41] It was found that the UV-Vis absorption and fluorescence emission spectra of QDs@SiO_2 nanobeads exhibited the same profiles as those of the hydrophobic QDs. The maximum absorption and emission peaks of QDs@SiO_2 nanobeads were located at 512 nm and 527 nm, respectively (Fig. 1A). Compared to hydrophobic QDs, the maximum emission of QDs@SiO_2 nanobeads showed a slight redshift, suggesting the high retention of the QD's original

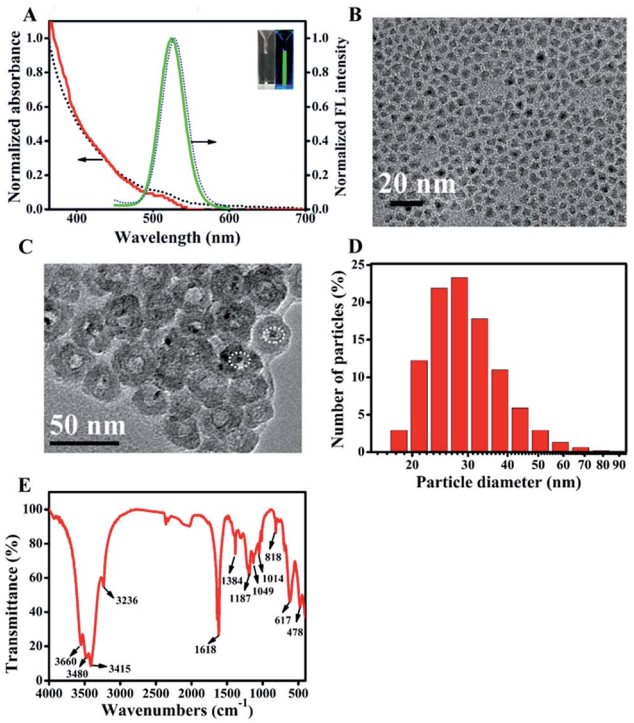

Fig. 1 (A) The UV-Vis absorption and fluorescence emission spectra of hydrophobic QDs (solid line) and QDs@SiO_2 nanobeads (dashed line). Inset: images of QDs@SiO_2 nanobeads in water under irradiation of sunlight (left) and UV lamp (right, 365 nm). (B) HRTEM image of the hydrophobic CdSe/ZnS QDs. (C) HRTEM image of the as-prepared QDs@SiO_2 nanobeads (the white dotted circles marked the position of QDs). (D) Size distribution of QDs@SiO_2 nanobeads. (E) FT-IR spectrum of QDs@SiO_2 nanobeads.

surface ligands after silication. The silica shell also preserved the intense fluorescence of hydrophobic QDs. Under the irradiation of a UV lamp, QDs@SiO_2 nanobeads emitted strong green fluorescence while the solution appeared almost colorless to the naked eye (inset images of Fig. 1A).

The photostability of QDs@SiO_2 nanobeads was studied to examine the effect of the silica shell. As demonstrated in Fig. S1,† when continuously excited for 70 min, the fluorescence intensity of the QDs@SiO_2 nanobeads did not show any degradation, indicating the high photostability of the incorporated QDs in aqueous media that resulted from the growth of the silica layer.

The morphology and size of the as-prepared QDs@SiO_2 nanobeads were characterized by HRTEM and dynamic light scattering (DLS) analysis. The HRTEM image (Fig. 1C) shows that the synthesized QDs@SiO_2 nanobeads were well dispersed and spherical in shape with a multicore–shell structure. The mean particle size of the QDs@SiO_2 nanobeads was calculated to be 28.0 ± 2.7 nm. For direct encapsulation of hydrophobic CdSe/ZnS QDs into silica beads, lipophilic silane was used to create micelles. Later, sodium silicate was introduced and deposited on the newly created micelles, causing a small increase in micelle size.[41] Thus, the average diameter of the QDs@SiO_2 nanobeads was much larger than that of the hydrophobic CdSe/ZnS QDs. DLS measurement (Fig. 1D) further revealed that the nanobeads exhibited a good size distribution in the range of 20–50 nm with an average size of 30.5 nm.

In order to study the interaction of QDs@SiO_2 nanobeads with MnO_2 nanosheets, the functional groups on the surface of the QDs@SiO_2 nanobeads were identified by FTIR spectrum (Fig. 1E). The characteristic absorption band centered at 3236 cm^{-1}, 3415 cm^{-1}, and 3480 cm^{-1} can be ascribed to the hydrogen-bonded O–H vibrations. The characteristic absorption peaks located at 818 cm^{-1} and 478 cm^{-1} confirmed the existence of SiO–H and Si–O groups.[59]

Zeta potential measurement is a useful tool for studying the surface charge of nanomaterials. To investigate the binding forces that might dominate the adhesion of the QDs@SiO_2 nanobeads to MnO_2 nanosheets, the zeta potential of QDs@SiO_2 nanobeads, MnO_2 nanosheets, and QDs@SiO_2@-MnO_2 nanocomposites was measured. As shown in Fig. S2,† the zeta potentials of the QDs@SiO_2 nanobeads and MnO_2 nanosheets were measured to be −46.7 ± 0.5 mV and −37.6 ± 0.4 mV, respectively, indicating the negative surface charge of the nanobeads and the nanosheets. After the QDs@SiO_2 nanobeads were modified with MnO_2 nanosheets, the value changed to −31.9 ± 0.2 mV. Although the QDs@SiO_2@MnO_2 nanocomposites were also negatively charged, the zeta potential value was lower than that of the nanobeads and the nanosheets, indicating the formation of the nanocomposites. Because the QDs@SiO_2 nanobeads and MnO_2 nanosheets were both negatively charged, electrostatic interaction was excluded. In addition, MnO_2 nanosheets could not provide π–π stacking with silanol groups.[60] Therefore, the assembly of MnO_2 nanosheets with QDs@SiO_2 nanobeads was possibly dominated by the coordination of deprotonated silanol groups with manganese ions. Furthermore, van der Waals forces between silanol groups and MnO_2 nanosheets may also play important roles in the adsorption process, which was similar to the result reported by another study.[60] Considering the results of FTIR spectrum and zeta potential measurements, the QDs@SiO_2 nanobeads may adhere to the surface of MnO_2 nanosheets by coordination and van der Waals forces.

Physical properties of MnO_2 nanosheets

As a promising energy acceptor, MnO_2 nanosheets can be facilely prepared through the reduction of $KMnO_4$ by MES. According to the TEM results (Fig. S3A†), it can be clearly seen that well-defined MnO_2 nanosheets with typical 2D morphology resulted from the reaction of $KMnO_4$ with MES.

The successful synthesis of MnO_2 nanosheets was further confirmed by the intense and broad characteristic absorption band around 380 nm (Fig. S3B†). Because the absorption spectrum of MnO_2 nanosheets overlaps well with the emission of QDs@SiO_2 nanobeads (Fig. S3B†), FRET may occur among the QDs@SiO_2@MnO_2 nanocomposites.

FRET between QDs@SiO_2 nanobeads and MnO_2 nanosheets

To achieve the best sensing performance, the molar ratio of QDs@SiO_2 nanobeads to MnO_2 nanosheets was optimized by

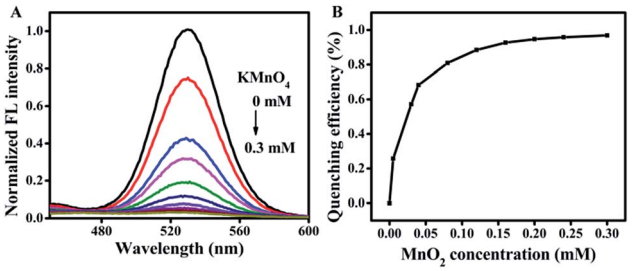

Fig. 2 (A) Fluorescence spectra of QDs@SiO_2 nanobeads under different concentrations of $KMnO_4$. (B) Fluorescence quenching efficiency of QDs@SiO_2 nanobeads *versus* concentrations of $KMnO_4$ (0, 0.0050, 0.030, 0.040, 0.080, 0.12, 0.16, 0.20, 0.24, and 0.30 mM).

adding different amounts of $KMnO_4$ to a fixed concentration of QDs@SiO_2 nanobeads. Fig. 2 reveals the FRET between the QDs@SiO_2 nanobeads and MnO_2 nanosheets. With the increasing concentrations of $KMnO_4$ (0 to 0.30 mM, the same concentration as the MnO_2 nanosheets) that were added, the fluorescence intensity of the QDs@SiO_2 nanobeads sharply decreased, indicating the strong quenching ability of MnO_2 nanosheets. As the concentration of $KMnO_4$ increased to 0.24 mM, a platform was reached, and a maximum fluorescence quenching efficiency of 96% was acquired. Further increase of acceptor concentration did not cause further fluorescence quenching, indicating the saturation of QDs@SiO_2 nanobeads by MnO_2 nanosheets. Therefore, 0.24 mM MnO_2 nanosheets *versus* 6.40 nM QDs@SiO_2 nanobeads was chosen for subsequent detection of GSH.

Validation of FRET

Fluorescence lifetime measurement is a useful tool for understanding the types of molecular interactions.[61] To prove the FRET between QDs@SiO_2 nanobeads and MnO_2 nanosheets, fluorescence lifetime measurements were performed. As shown in Fig. 3A, the decay curves of QDs@SiO_2 nanobeads in the absence and presence of MnO_2 nanosheets were well-fitted with a biexponential function. Upon addition of MnO_2 nanosheets, the fluorescence lifetime of QDs@SiO_2 nanobeads decreased from 19.54 ns to 14.25 ns, implying that the observed quenching was mainly induced by a FRET process.

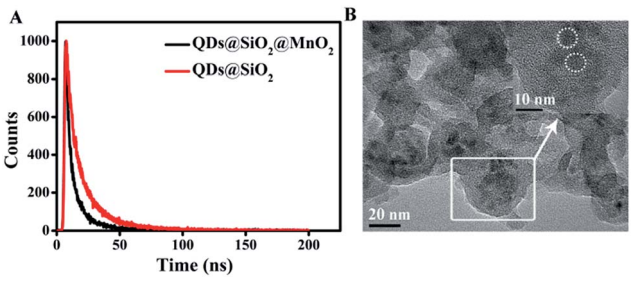

Fig. 3 (A) Fluorescence decay curves of QDs@SiO_2 nanobeads in the absence and presence of MnO_2 nanosheets. The concentrations of QDs@SiO_2 nanobeads and MnO_2 nanosheets were fixed at 69 nM and 0.29 mM respectively. (B) HRTEM image of QDs@SiO_2@MnO_2 nanocomposites (inset: enlarged photograph of a single QDs@SiO_2 nanobead). The white dotted circles denote a single QD.

To further confirm the FRET between the QDs@SiO_2 nanobeads and MnO_2 nanosheets, the morphology of the QDs@SiO_2@MnO_2 nanocomposites was studied by HRTEM (Fig. 3B). The results showed that QDs@SiO_2 nanobeads were well dispersed on the surface of the MnO_2 nanosheets. In the absence of the QDs@SiO_2 nanobeads, the MnO_2 nanosheets tended to aggregate and formed a dark brown precipitate. Once the QDs@SiO_2 nanobeads were added, a colloidal solution was obtained due to the excellent water solubility of the nanobeads. The HRTEM results also indicated that the *in situ* synthesis of the MnO_2 nanosheets did not have any negative effect on the shape or size of the nanobeads, as the morphology of the QDs was well-resolved (inset image of Fig. 3B).

In addition, to validate the modification of the QDs@SiO_2 nanobeads by MnO_2 nanosheets, the composition of QDs@SiO_2@MnO_2 nanocomposites was characterized by X-ray photoelectron spectroscopy (XPS) and energy dispersive X-ray spectroscopy (EDS). The full range XPS spectrum of QDs@SiO_2 nanobeads distinctly indicated the presence of elemental Cd, Se, Zn, S, Si, and O (Fig. S4A†). Compared with pure QDs@SiO_2 nanobeads, an additional Mn 2p peak was observed in the spectrum of the QDs@SiO_2@MnO_2 nanocomposites, suggesting that the QDs@SiO_2 nanobeads were successfully modified with MnO_2 nanosheets. The high resolution spectrum of Mn 2p exhibited two sharp peaks at 641.9 eV and 653.4 eV (Fig. S4B†), which were assigned to Mn $2p_{3/2}$ and Mn $2p_{1/2}$, respectively. The spin-energy separation of 11.5 eV indicated that the predominant oxidation state of Mn in MnO_2 nanosheets is +4.[62] The compositional analysis by EDS also proved that QDs@SiO_2 nanobeads were successfully modified with MnO_2 nanosheets, and they assembled to one sample as a probe (Fig. S5†).

Dominated by coordination and van der Waals forces, the QDs@SiO_2 nanobeads adhered to the surface of the MnO_2 nanosheets and brought them into proximity. As a result, FRET occurred *via* the dipole–dipole interaction, and the fluorescence intensity of the QDs@SiO_2 nanobeads was intensely quenched by the MnO_2 nanosheets.

Detection of GSH

At the optimum molar ratio of QDs@SiO_2 nanobeads to MnO_2 nanosheets, the constructed FRET probe was applied to detect the concentrations of GSH in aqueous solution. To explore this sensing platform, the reaction time of the QDs@SiO_2@MnO_2 nanocomposites with GSH was optimized and was selected as 16 min (Fig. S6†). As shown in Fig. 4A, upon the addition of GSH, the fluorescence intensity of QDs@SiO_2 nanobeads remarkably recovered, indicating the elimination of FRET that resulted from an oxidation–reduction process. In the presence of GSH, MnO_2 was reduced to Mn^{2+} ions and GSH itself was oxidized to glutathione disulfide (GSSG), leading to a disappearance of MnO_2 nanosheets, and thus resulted in a fluorescence recovery of QDs@SiO_2 nanobeads.

As the concentration of GSH reached 0.48 mM, *i.e.*, 2-fold of the MnO_2 nanosheets, a maximum enhancement of

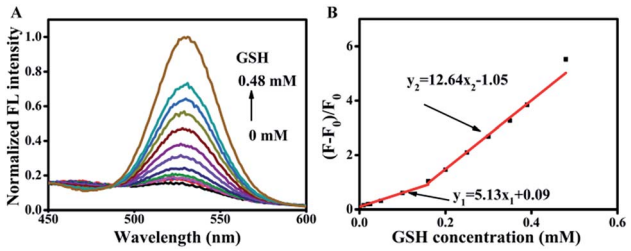

Fig. 4 (A) Fluorescence spectra of QDs@SiO_2@MnO_2 nanocomposites (6.40 nM QDs@SiO_2 nanobeads *versus* 0.24 mM MnO_2 nanosheets) in the presence of different concentrations of GSH (0 to 0.48 mM). (B) Linear fit of the fluorescence enhancement ratio to the concentrations of GSH. Each experiment was repeated three times.

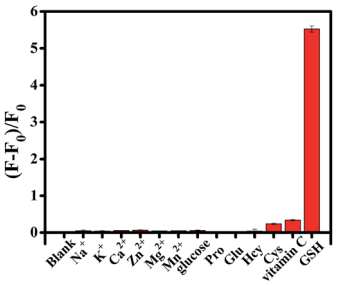

Fig. 5 Fluorescence response of QDs@SiO_2@MnO_2 nanocomposites to GSH and other potential interferences.

fluorescence intensity was achieved. But further increase in the GSH concentration did not cause further fluorescence enhancement. This observation perfectly agreed with the reaction mechanism that two moles of GSH can reduce one mole of MnO_2.[16] The fluorescence enhancement ratio, $(F - F_0)/F_0$ (F_0 represents the fluorescence intensity of QDs@SiO_2@MnO_2 nanocomposites in the absence of GSH and F represents the fluorescence intensity under different concentrations of GSH), was calculated and was found to be linear to the concentration of GSH. It is worth noting that the dependence of $(F - F_0)/F_0$ on GSH concentration followed two equations in two different concentration ranges (Fig. 4B). One is

$(F - F_0)/F_0 = 5.13$ [GSH] + 0.09 ($R = 0.9844$ and [GSH] denotes the concentration of GSH), (1)

with the concentrations of GSH ranging from 0.010 to 0.16 mM and the other one is

$$(F - F_0)/F_0 = 12.64 \text{ [GSH]} - 1.05 \ (R = 0.9951), \quad (2)$$

with the concentrations of GSH from 0.16 mM to 0.48 mM. The difference in slopes in the two GSH concentration ranges might result from the diverse reaction states of QDs@SiO_2@MnO_2 nanocomposites with GSH. In the previous experiment, in order to achieve a maximum fluorescence quenching efficiency, the concentration of MnO_2 nanosheets was set as 0.24 mM. Therefore, at lower GSH concentrations, the QDs@SiO_2 nanobeads were tightly coated with large amounts of MnO_2 nanosheets. The added GSH can simply reduce a small amount of them, and the fluorescence recovery was not so effective as expected. According to the obtained linear relationship, the limit of detection (LOD) was determined to be 0.61 μM based on the $3\sigma/s$ method, where σ is the standard deviation of blank signals ($n = 11$) and s is the slope of eqn (1). The results indicated that the sensing performance of this rationally designed FRET-based probe is favorable and comparable to other materials previously reported,[16,58] and it has great potential for quantitative analysis of GSH.

Selectivity studies for GSH

Specific recognition of the target is an essential feature of a probe. Therefore, the specificity of the probe towards GSH and other potential interferences of many species, involving metal ions (Na^+, K^+, Ca^{2+}, Zn^{2+}, Mg^{2+}, and Mn^{2+}), amino acids (Glu, Pro, Hcy, and Cys), glucose, and vitamin C, were examined. When the QDs@SiO_2@MnO_2 nanocomposites were incubated with the above species, no obvious fluorescence enhancement was observed from the interferences, and only GSH could cause remarkable fluorescence recovery (Fig. 5). Reducing agents, such as Cys, Hcy, and vitamin C, could also react with the MnO_2 nanosheets and induce fluorescence recovery, but their amounts in human blood are much lower than that of GSH.[50] Therefore, QDs@SiO_2@MnO_2 nanocomposites represent a high selectivity towards GSH and ensure the highly selective detection of GSH in a complex matrix.

Table 1 Determination of GSH in reduced glutathione tablets

Measured (mM)	Added (mM)	Found (mM)	RSD (%)	Recovery (%)
0.164	0.100	0.254	1.5	90.0
	0.200	0.341	1.7	88.5

Pharmaceutical analysis

To illustrate the feasibility of our probe for GSH detection in a complex matrix, the content of GSH in reduced glutathione tablets was analyzed. According to the calibration curve established in Fig. 4B, the content of GSH in reduced glutathione tablets was calculated to be 104.3%, which was consistent with the labeled content of reduced glutathione tablets. The recoveries of GSH in reduced glutathione tablets were also tested by the standard addition method. As displayed in Table 1, excellent recoveries of 88.5% and 90.0% were obtained with an RSD that was lower than 1.7%. The above results show the capability of the probe to detect lower concentrations of GSH and indicate the practicability of the probe for GSH determination in real samples.

Conclusions

In summary, a simple, sensitive, selective, rapid, and label-free FRET-based probe for GSH using MnO_2 nanosheets as an energy acceptor and CdSe/ZnS QDs as an energy donor was rationally designed. The direct encapsulation of hydrophobic

QDs into silica beads can provide QDs with good biocompatibility, highly preserved fluorescence, and robust chemical and photochemical stability. The *in situ* synthesis of MnO_2 nanosheets was facile and effective, and a maximum fluorescence quenching efficiency of 96% was achieved. The established FRET sensing probe can respond to GSH in aqueous solution within the range of 0.010 to 0.48 mM. The detection limit was calculated to be 0.61 μM, indicating the high sensitivity of the probe for GSH. The probe also showed excellent selectivity towards GSH among other interference species and could be used to detect GSH in a complex matrix of reduced glutathione tablets with satisfactory recoveries. The results of this work indicate the capability of this approach for GSH detection both in aqueous solutions and real samples. In addition, it provides new insights into the interactions of QDs with 2D-GAs and promotes their applications in bioassays.

Conflicts of interest

There are no conflicts of interest to declare.

Acknowledgements

The authors gratefully acknowledge the financial support from the National Natural Science Foundation of China (grant number 21205043) and Da Bei Nong Group Promoted Project for Young Scholar of HZAU (grant number 2017DBN009).

Notes and references

1 H. J. Forman, H. Zhang and A. Rinna, *Mol. Aspects Med.*, 2009, **30**, 1–12.
2 S. C. Lu, *Mol. Aspects Med.*, 2009, **30**, 42–59.
3 H. L. Martin and P. Teismann, *FASEB J.*, 2009, **23**, 3263–3272.
4 C. B. Pocernich and D. A. Butterfield, *Biochim. Biophys. Acta, Mol. Basis Dis.*, 2012, **1822**, 625–630.
5 D. M. Townsend, K. D. Tew and H. Tapiero, *Biomed. Pharmacother.*, 2003, **57**, 145–155.
6 Y. Wang, L. Jiang, L. Chu, W. Liu, S. Wu, Y. Wu, X. He and K. Wang, *Biosens. Bioelectron.*, 2017, **87**, 459–465.
7 W. Wang, L. Zhang, L. Li and Y. Tian, *Anal. Chem.*, 2016, **88**, 9518–9523.
8 Y. Wang, J. Lu, L. Tang, H. Chang and J. Li, *Anal. Chem.*, 2009, **81**, 9710–9715.
9 J. Yu, C. Li, S. Shen, X. Liu, Y. Peng and J. Zheng, *Rapid Commun. Mass Spectrom.*, 2015, **29**, 681–689.
10 X.-F. Yang, Q. Huang, Y. Zhong, Z. Li, H. Li, M. Lowry, J. O. Escobedo and R. M. Strongin, *Chem. Sci.*, 2014, **5**, 2177–2183.
11 N. Uehara, K. Ookubo and T. Shimizu, *Langmuir*, 2010, **26**, 6818–6825.
12 Z.-M. Huang, Q.-Y. Cai, D.-C. Ding, J. Ge, Y.-L. Hu, J. Yang, L. Zhang and Z.-H. Li, *Sens. Actuators, B*, 2017, **242**, 355–361.
13 X. Chen, Y. Zhou, X. Peng and J. Yoon, *Chem. Soc. Rev.*, 2010, **39**, 2120–2135.
14 J. Yin, Y. Kwon, D. Kim, D. Lee, G. Kim, Y. Hu, J. H. Ryu and J. Yoon, *J. Am. Chem. Soc.*, 2014, **136**, 5351–5358.
15 J. Liu, C. Bao, X. Zhong, C. Zhao and L. Zhu, *Chem. Commun.*, 2010, **46**, 2971–2973.
16 R. Deng, X. Xie, M. Vendrell, Y.-T. Chang and X. Liu, *J. Am. Chem. Soc.*, 2011, **133**, 20168–20171.
17 X. Yan, Y. Song, C. Zhu, J. Song, D. Du, X. Su and Y. Lin, *ACS Appl. Mater. Interfaces*, 2016, **8**, 21990–21996.
18 Q.-Y. Cai, J. Li, J. Ge, L. Zhang, Y.-L. Hu, Z.-H. Li and L.-B. Qu, *Biosens. Bioelectron.*, 2015, **72**, 31–36.
19 C. Li and C. Wei, *Sens. Actuators, B*, 2017, **240**, 451–458.
20 S. Xu, T. Gao, X. Feng, Y. Mao, P. Liu, X. Yu and X. Luo, *J. Mater. Chem. B*, 2016, **4**, 1270–1275.
21 U. Resch-Genger, M. Grabolle, S. Cavaliere-Jaricot, R. Nitschke and T. Nann, *Nat. Methods*, 2008, **5**, 763–775.
22 Y. Du and S. Guo, *Nanoscale*, 2016, **8**, 2532–2543.
23 S. Y. Lim, W. Shen and Z. Gao, *Chem. Soc. Rev.*, 2015, **44**, 362–381.
24 M. F. Frasco and N. Chaniotakis, *Sensors*, 2009, **9**, 7266–7286.
25 K. E. Sapsford, T. Pons, I. L. Medintz and H. Mattoussi, *Sensors*, 2006, **6**, 925–953.
26 X. Gao, Y. Cui, R. M. Levenson, L. W. K. Chung and S. Nie, *Nat. Biotechnol.*, 2004, **22**, 969–976.
27 A. C. S. Samia, X. Chen and C. Burda, *J. Am. Chem. Soc.*, 2003, **125**, 15736–15737.
28 D. J. Mowbray and M. S. Skolnick, *J. Phys. D: Appl. Phys.*, 2005, **38**, 2059–2076.
29 X. Ji, J. Zheng, J. Xu, V. K. Rastogi, T. C. Cheng, J. J. DeFrank and R. M. Leblanc, *J. Phys. Chem. B*, 2005, **109**, 3793–3799.
30 Y. Ebenstein, T. Mokari and U. Banin, *J. Phys. Chem. B*, 2004, **108**, 93–99.
31 E. R. Goldman, E. D. Balighian, H. Mattoussi, M. K. Kuno, J. M. Mauro, P. T. Tran and G. P. Anderson, *J. Am. Chem. Soc.*, 2002, **124**, 6378–6382.
32 L. E. Page, X. Zhang, A. M. Jawaid and P. T. Snee, *Chem. Commun.*, 2011, **47**, 7773–7775.
33 T.-W. Sung and Y.-L. Lo, *Sens. Actuators, B*, 2012, **165**, 119–125.
34 C.-P. Huang, Y.-K. Li and T.-M. Chen, *Biosens. Bioelectron.*, 2007, **22**, 1835–1838.
35 G. M. Durán, A. M. Contento and Á. Ríos, *Anal. Chim. Acta*, 2013, **801**, 84–90.
36 M.-C. Tu, Y.-T. Chang, Y.-T. Kang, H.-Y. Chang, P. Chang and T.-R. Yew, *Biosens. Bioelectron.*, 2012, **34**, 286–290.
37 S. Raichlin, E. Sharon, R. Freeman, Y. Tzfati and I. Willner, *Biosens. Bioelectron.*, 2011, **26**, 4681–4689.
38 A. M. Derfus, W. C. W. Chan and S. N. Bhatia, *Nano Lett.*, 2004, **4**, 11–18.
39 F. Dubois, B. Mahler, B. Dubertret, E. Doris and C. Mioskowski, *J. Am. Chem. Soc.*, 2007, **129**, 482–483.
40 C.-A. J. Lin, R. A. Sperling, J. K. Li, T. Y. Yang, P.-Y. Li, M. Zanella, W. H. Chang and W. J. Parak, *Small*, 2008, **4**, 334–341.
41 L. Huang, Z. Luo and H. Han, *Chem. Commun.*, 2012, **48**, 6145–6147.
42 L. Chen and H. Han, *Microchim. Acta*, 2014, **181**, 1485–1495.
43 Y. Chen, C. Tan, H. Zhang and L. Wang, *Chem. Soc. Rev.*, 2015, **44**, 2681–2701.

44 Y. Omomo, T. Sasaki, L. Wang and M. Watanabe, *J. Am. Chem. Soc.*, 2003, **125**, 3568–3575.
45 C. Wang, W. Zhai, Y. Wang, P. Yu and L. Mao, *Analyst*, 2015, **140**, 4021–4029.
46 J. Yuan, Y. Cen, X. J. Kong, S. Wu, C.-L. Liu, R.-Q. Yu and X. Chu, *ACS Appl. Mater. Interfaces*, 2015, **7**, 10548–10555.
47 X.-L. Zhang, C. Zheng, S.-S. Guo, J. Li, H.-H. Yang and G. Chen, *Anal. Chem.*, 2014, **86**, 3426–3434.
48 Y. Wang, K. Jiang, J. Zhu, L. Zhang and H. Lin, *Chem. Commun.*, 2015, **51**, 12748–12751.
49 Y. Xu, X. Chen, R. Chai, C. Xing, H. Li and X.-B. Yin, *Nanoscale*, 2016, **8**, 13414–13421.
50 S. Lin, H. Cheng, Q. Ouyang and H. Wei, *Anal. Methods*, 2016, **8**, 3935–3940.
51 H.-B. Wang, Y. Chen, N. Li and Y.-M. Liu, *Microchim. Acta*, 2017, **184**, 515–523.
52 Q. Cai, L. Zhang, X. Geng, J. Ge and Z. Li, *J. Nanosci. Nanotechnol.*, 2018, **18**, 1709–1715.
53 J. Chen, Z. Huang, H. Meng, L. Zhang, D. Ji, J. Liu, F. Yu, L. Qu and Z. Li, *Sens. Actuators, B*, 2018, **260**, 770–777.
54 Y.-L. Xu, X.-Y. Niu, H.-L. Chen, S.-G. Zhao and X.-G. Chen, *Chin. Chem. Lett.*, 2017, **28**, 338–344.
55 H. Ma, X. Li, X. Liu, M. Deng, X. Wang, A. Iqbal, W. Liu and W. Qin, *Sens. Actuators, B*, 2018, **255**, 1687–1693.
56 N. Li, W. Diao, Y. Han, W. Pan, T. Zhang and B. Tang, *Chem.–Eur. J.*, 2014, **20**, 16488–16491.
57 W. W. Yu, L. Qu, W. Guo and X. Peng, *Chem. Mater.*, 2003, **15**, 2854–2860.
58 Z. Liu, X. Cai, X. Lin, Y. Zheng, Y. Wu, P. Chen, S. Weng, L. Lin and X. Lin, *Anal. Methods*, 2016, **8**, 2366–2374.
59 T. Qian, J. Li, H. Ma and J. Yang, *Sol. Energy Mater. Sol. Cells*, 2015, **132**, 29–39.
60 Y. Yuan, S. Wu, F. Shu and Z. Liu, *Chem. Commun.*, 2014, **50**, 1095–1097.
61 J. R. Lakowicz, *Principles of Fluorescence Spectroscopy*, Springer Academic, New York, 2006, pp. 277–330.
62 W.-J. Lu, S.-Z. Huang, L. Miao, M.-X. Liu, D.-Z. Zhu, L.-C. Li, H. Duan, Z.-J. Xu and L.-H. Gan, *Chin. Chem. Lett.*, 2017, **28**, 1324–1329.